Composite synoptic-scale environments conducive to North American polar–subtropical jet superposition events

By

ANDREW C. WINTERS[1*], DANIEL KEYSER[2], LANCE F. BOSART[2], and JONATHAN E. MARTIN[3]

[1]Department of Atmospheric and Oceanic Sciences
University of Colorado Boulder
Boulder, CO 80309

[2]Department of Atmospheric and Environmental Sciences
University at Albany, State University of New York
Albany, NY 12222

[3]Department of Atmospheric and Oceanic Sciences
University of Wisconsin–Madison
Madison, WI 53706

Submitted for publication in *Monthly Weather Review*
XX October 2019

[*] *Corresponding author address:* Andrew C. Winters, Dept. of Atmospheric and Oceanic Sciences, University of Colorado Boulder, UCB 311, Boulder, CO 80309. E-mail: andrew.c.winters@colorado.edu

ABSTRACT

The development of a polar–subtropical jet superposition establishes a dynamical and thermodynamic environment that is conducive to the production of high-impact weather. Prior work indicates that the synoptic-scale environments that support the development of North American jet superpositions can vary considerably depending on the case under consideration. This variability motivates a comprehensive examination of the range of synoptic-dynamic mechanisms that operate within a double-jet environment to produce North American jet superpositions. This study objectively identifies North American jet superposition events during November–March 1979–2010 and subsequently classifies those events into three characteristic event types. "Polar dominant" events are those during which only the polar jet is characterized by a substantial excursion from its climatological latitude band, "subtropical dominant" events are those during which only the subtropical jet is characterized by a substantial excursion from its climatological latitude band, and "hybrid" events are those characterized by a mutual excursion of both jets from their respective climatological latitude bands. The analysis indicates that North American jet superposition events occur most often during November and December, and that subtropical dominant events are the most frequent event type. Composite analyses constructed for each jet superposition event type reveal the common role that descent plays in restructuring the tropopause beneath the confluent jet-entrance region prior to each event type. The composite analyses further show that surface cyclogenesis and widespread precipitation tend to lead the development of subtropical dominant events, while surface cyclogenesis and widespread precipitation tend to be maximized concurrently with and downstream of polar dominant events.

1. Introduction

The instantaneous positions of the polar and subtropical jets are closely related to the pole-to-equator tropopause structure, as indicated by the idealized vertical cross section provided in Fig. 1a. In the Northern Hemisphere, the average location of the polar jet is near 50°N in the region where the tropopause height abruptly rises from the polar tropopause (~350 hPa) to the subtropical tropopause (~250 hPa). The polar jet also resides atop the strongly baroclinic and tropospheric-deep polar front (e.g., Palmén and Newton 1948; Namias and Clapp 1949; Newton 1954; Palmén and Newton 1969, Keyser and Shapiro 1986; Shapiro and Keyser 1990). The average position of the subtropical jet is located equatorward of the polar jet near 30°N in the region where the tropopause height abruptly rises from the subtropical tropopause (~250 hPa) to the tropical tropopause (~100 hPa). In contrast to the polar jet, the subtropical jet is characterized by relatively modest baroclinicity in the upper troposphere and lower stratosphere (e.g., Starr 1948; Loewe and Radok 1950; Yeh 1950; Koteswaram 1953; Mohri 1953; Koteswaram and Parthasarathy 1954; Sutcliffe and Bannon 1954; Krishnamurti 1961; Riehl 1962).

While the polar and subtropical jets typically occupy separate climatological latitude bands, the latitudinal separation between the two jet streams occasionally vanishes, resulting in a vertical superposition of the polar and subtropical jets (e.g., Winters and Martin 2014, 2016, 2017; Handlos and Martin 2016; Christenson et al. 2017). An idealized vertical cross section perpendicular to the axis of a jet superposition is shown in Fig. 1b and reveals the principal characteristics of a jet superposition. These characteristics include the development of (1) a steep, two-step pole-to-equator tropopause structure, (2) anomalously strong wind speeds that can exceed 100 m s^{-1} in some instances, and (3) strong baroclinicity in the upper troposphere and lower stratosphere as required by thermal wind balance. The development of strong baroclinicity in association with the jet superposition is also accompanied by the formation of a vigorous across-front ageostrophic circulation that can directly influence the production of high-impact weather (e.g., Winters and Martin 2014, 2016, 2017).

A climatological survey of Northern Hemisphere jet superposition events constructed by Christenson et al. (2017) using the NCEP–NCAR Reanalysis dataset (Kalnay et al. 1996; Kistler et al. 2001) during November–March 1960–2010 indicates that jet superpositions are most frequent over the western North Pacific, North America, and northern Africa. The key dynamical processes associated with western North Pacific jet superpositions, in particular, have been examined in detail by Handlos and Martin (2016). These dynamical processes include equatorward surges of lower-tropospheric cold air over the east Asian continent that act to strengthen the lower-tropospheric baroclinicity at middle and subtropical latitudes, and the development of widespread convection over the equatorial western North Pacific.

Prior work concerning North American jet superpositions has focused solely on individual case studies. Winters and Martin (2014, 2016) examined the development of a jet superposition within a highly amplified upper-tropospheric flow pattern during the 1–3 May 2010 Tennessee Flood, and determined that a substantial fraction of the poleward moisture transport into the southeastern U.S. prior to the second day of the event was attributable to the across-front ageostrophic circulation associated with the superposed jet. This poleward moisture transport ensured that widespread precipitation continued throughout the second day of the event (Moore et al. 2012). Furthermore, the presence of widespread precipitation during the May 2010 Tennessee Flood contributed to the diabatic erosion of upper-tropospheric potential vorticity (PV) on the equatorward side of the subtropical jet and strong negative PV advection by the irrotational wind along the axis of the subtropical jet. These two processes facilitated a substantial poleward shift in the position of the subtropical waveguide and the formation of the steep, two-step tropopause structure that accompanied the jet superposition.

Winters and Martin (2016, 2017) performed a complementary analysis of a wintertime jet superposition event on 20 December 2009 that featured a rapidly deepening surface cyclone beneath the poleward-exit region of the superposed jet. This cyclone was associated with snowfall totals in excess of 30 cm (~12 in.) in locations ranging from the Mid-Atlantic northeastward towards New England. In contrast to the May 2010 Tennessee Flood, widespread precipitation on the equatorward side of the subtropical jet did not play a substantial role in facilitating the development of the two-step tropopause structure within the superposed jet during the December 2009 case. Instead, Winters and Martin (2016, 2017) determined that the descending branch of an across-front ageostrophic circulation within the double-jet environment played the dominant role in restructuring the tropopause prior to superposition.

The two aforementioned cases served as the foundation for the conceptual model of North American jet superpositions (Fig. 1c) introduced by Winters and Martin (2017; their Fig. 2). In this model, jet superposition features the development of a polar cyclonic PV anomaly at high latitudes with a polar jet located equatorward of the PV anomaly. Polar cyclonic PV anomalies, which include coherent tropopause disturbances (e.g., Hakim 2000; Pyle et al. 2004) and tropopause polar vortices (e.g., Cavallo and Hakim 2009, 2010, 2012, 2013), typify a dynamical environment that can be particularly conducive to surface cyclogenesis at middle and high latitudes (e.g., Hakim et al. 1995, 1996; Pyle et al. 2004; Cavallo and Hakim 2010).

Jet superposition also features the concomitant production of a tropical anticyclonic PV anomaly on the equatorward side of the subtropical jet. Tropical anticyclonic PV anomalies result from the poleward transport of tropical, low-PV upper-tropospheric air via low-latitude troughs and tropical plumes (e.g., Iskenderian 1995; Roundy et al. 2010; Fröhlich et al. 2013; Winters and Martin 2016), and/or tropical cyclones (e.g., McTaggart-Cowan et al. 2007; Archambault et al. 2013, 2015). Tropical anticyclonic PV anomalies at middle latitudes typify a thermodynamic environment characterized by weak upper-tropospheric static stability, and can be accompanied by an atmospheric river (e.g., Newell et al. 1992; Zhu and Newell 1998; Ralph et al. 2004, 2018, 2019) within the poleward-directed branch of the tropospheric-deep, nondivergent circulation induced by the anticyclonic PV anomaly.

If polar cyclonic and tropical anticyclonic PV anomalies are situated within a confluent large-scale flow pattern and phase favorably, the result is a meridional juxtaposition of the respective PV anomalies at middle latitudes. This configuration encourages constructive interference between the nondivergent circulations induced by each PV anomaly and a rapid increase in wind speed in the area between the two anomalies. The meridional juxtaposition of the respective PV anomalies also establishes a dynamical and thermodynamic environment that is particularly conducive to high-impact weather.

Once the respective PV anomalies are meridionally juxtaposed, mesoscale processes within the near-jet environment act to restructure the tropopause to produce the steep, two-step tropopause structure that accompanies a jet superposition (i.e., Fig. 1b). Mesoscale processes capable of restructuring the tropopause within a double-jet environment include across-front ageostrophic circulations (e.g., Shapiro 1981, 1982; Keyser and Pecnick 1985; Keyser and Shapiro 1986; Lang and Martin 2012; Martin 2014; Handlos and Martin 2016; Winters and Martin, 2016, 2017), as well as the diabatic heating and negative PV advection by the irrotational wind along the dynamic tropopause that accompany areas of widespread precipitation (e.g., Lee and Kim 2003; Agustí-Panareda et al. 2004; Ahmadi-Givi et al. 2004; Son and Lee 2005; Grams et al. 2011, 2013; Archambault et al. 2013, 2015; Lang and Martin 2013; Grams and Archambault 2016; Handlos and Martin 2016; Winters and Martin 2016, 2017). The aforementioned mesoscale processes also contribute to the rapid increase in wind speed observed in conjunction with the jet superposition.

While the conceptual model presented in Fig. 1c generalizes the process of jet superposition over North America, it does not reveal the degree to which the dynamical processes responsible for producing a jet superposition (i.e., across-front ageostrophic circulations, diabatic heating, and negative PV advection by the irrotational wind) vary between jet superposition events (e.g., Winters and Martin 2016; 2017). Furthermore, the conceptual model in Fig. 1c does not portray the spectrum of interactions that can occur between polar cyclonic and tropical anticyclonic PV anomalies prior to jet superposition. For instance, an individual jet superposition can arise solely in response to a substantial equatorward deviation of the polar jet towards the latitude of the subtropical jet, and vice versa. To address these shortcomings, this study adopts a comprehensive approach to characterize the variability of North American jet superpositions, and to reveal the spectrum of dynamical processes and synoptic-scale evolutions that lead to North American jet superpositions.

The remainder of this study is structured as follows. Section 2 introduces the objective identification scheme used to identify jet superposition events and the classification scheme employed to partition jet superposition events into event types. Section 3 discusses the climatological characteristics of each jet superposition event type. Section 4 discusses the composite synoptic-scale flow evolutions associated with selected jet superposition event types, and section 5 summarizes the results.

2. Data and Methodology

This study employs data from the 0.5°-resolution National Centers for Environmental Prediction Climate Forecast System Reanalysis (CFSR; Saha et al. 2010) at 6-h intervals during November–March 1979–2010. This temporal period is chosen to ensure that the forthcoming analysis overlaps entirely with the period examined in Christenson et al. (2017). The CFSR is chosen to obtain a finer resolution of the dynamical evolutions that precede jet superpositions than the coarser NCEP–NCAR reanalysis dataset used in prior examinations of superpositions (e.g., Handlos and Martin 2016; Christenson et al. 2017). All CFSR data were bilinearly interpolated onto isentropic surfaces between 300 K and 380 K at 5-K intervals to accommodate the forthcoming jet superposition identification scheme. This study also utilizes the 2.5°-resolution NOAA Interpolated Outgoing Longwave Radiation (OLR) dataset (Liebmann and Smith 1996) to construct daily composites of OLR for each jet superposition event type. Areas characterized by negative OLR anomalies serve as proxies for the location of extensive cloud cover, and may imply the presence of precipitation if the OLR anomalies overlap with a favorable dynamic and thermodynamic environment for large-scale ascent.

a) Jet Superposition Event Identification

The objective jet superposition identification scheme used in this study is identical to that described in Winters and Martin (2014, 2016), Handlos and Martin (2016), and Christenson et al. (2017). While the forthcoming discussion provides a brief conceptual overview of the identification scheme, the reader is referred to the aforementioned studies for additional detail.

The jet identification scheme is grid-column based, in that the scheme identifies grid columns in the CFSR that exhibit the characteristics of a polar or a subtropical jet. A polar (subtropical) jet is identified at a grid column if two criteria are satisfied. First, the integrated wind speed within that grid column must exceed 30 m s^{-1} within the 400–100-hPa layer. Second, the magnitude of the horizontal PV gradient within the 1–3-PVU channel at that grid column must exceed an empirically-defined threshold[1] in the 315–330-K (340–355-K) isentropic layer. As implied by Fig. 1a, a strong horizontal PV gradient in the 315–330-K (340–355-K) isentropic layer physically corresponds to the presence of a discontinuity between the polar and subtropical tropopauses (subtropical and tropical tropopauses). The identification of a polar and a subtropical jet within the same grid column of CFSR data at a single analysis time results in the identification of a jet superposition at that grid column, and is interpreted physically as the formation of a steep, two-step tropopause structure (i.e., Fig. 1b). On a horizontal map, this scheme is manifest at a single analysis time as a ribbon of positively-identified grid columns that parallel the axis of a superposed jet (not shown).

North American jet superpositions were isolated during the cold season (November–March) for this study within a domain bounded in latitude from 10° to 80°N and in longitude from 140°W to 50°W. While jet superpositions do occur outside of the cold season (e.g., the May 2010 Tennessee Flood), the aforementioned jet identification scheme would need to be modified to account for the seasonal variability of the isentropic layers that house the polar and subtropical jets in order to identify jet superpositions outside of the cold season. An investigation into the character of North American jet superpositions outside of the cold season is outside of the scope of the present study and is reserved for future work.

Following their identification, all 6-h analysis times characterized by a jet superposition were filtered to retain only those times that rank in the top 10% in terms of the number of grid columns characterized by a jet superposition (i.e., those analysis times that featured 18 or more

[1] The specific threshold used for the magnitude of the horizontal PV gradient within the 315–330-K (340–355-K) isentropic layer is 1.4×10^{-5} PVU m^{-1} (0.9×10^{-5} PVU m^{-1}), where 1 PVU = 10^{-6} K m^2 kg^{-1} s^{-1}.

grid columns characterized by a jet superposition). This filter retains only those analysis times in which the polar and subtropical jets are vertically superposed along a substantial length of the jet axis. All grid columns characterized by a jet superposition during a retained analysis time were also required to be located within 1000 km of another grid column characterized by a superposition. If an analysis time featured a group of 18 or more grid columns that satisfied this distance criterion, it was labeled a "jet superposition event". Although rare, this methodology allows for the identification of multiple jet superposition events at a single analysis time, so long as the groups of jet superposition grid columns are more than 1000 km apart and each group is at least 18 grid columns in size.

The latitude and longitude of each grid column associated with a single jet superposition event were averaged to compute a latitude-longitude centroid for that particular event. The positions of the jet superposition event centroids were then compared across all events to group together jet superposition events that may be associated with the same jet. In particular, if an event centroid during one event was located within 1500 km of the location of another event centroid during the previous 30-h period, those jet superposition events were considered to be the same event. The methodology described above produced a total of 326 jet superposition events.

b) Jet Superposition Event Classification

Following their identification, jet superposition events were classified into event types based on the degree to which the polar and subtropical jets deviated from their respective climatological positions to form a jet superposition. The climatological position of the polar (subtropical) waveguide at a single analysis time (e.g., 0000 UTC 1 January) was calculated by averaging the position of the 2-PVU contour on the 320-K (350-K) isentropic surface at 24-h intervals within a 21-day window centered on that analysis time for every year between 1979 and

2010. The 320- and 350-K isentropes reside firmly within the isentropic layers used to identify the polar and subtropical jets, respectively, and serve as reasonable proxies for the positions of the polar and subtropical waveguides during the cold season (e.g., Martius et al. 2010; Christenson et al. 2017).

The event classification scheme subsequently compares the position of each jet superposition event centroid against the climatological positions of both the polar and subtropical waveguides at the start of an event. “Polar dominant” events (Fig. 2a) are those events in which an observation of 2 PVU at the location of the event centroid represents a standardized PV anomaly > 0.5 on the 320-K isentropic surface and a standardized PV anomaly > –0.5 on the 350-K isentropic surface. Consequently, polar dominant events exhibit a substantial equatorward deviation of the polar jet from its climatological position to superpose with the subtropical jet near its climatological position. “Hybrid” events (Fig. 2b) are those events in which an observation of 2 PVU at the location of the event centroid represents a standardized PV anomaly > 0.5 on the 320-K isentropic surface and a standardized PV anomaly < –0.5 on the 350-K isentropic surface. Hybrid events, therefore, exhibit a mutual deviation of the polar and subtropical jets from their respective climatological positions to form a superposition. “Subtropical dominant” events (Fig. 2c) are those events in which an observation of 2 PVU at the location of the event centroid represents a standardized PV anomaly < 0.5 on the 320-K isentropic surface and a standardized PV anomaly < –0.5 on the 350-K isentropic surface. Subtropical dominant events exhibit a substantial poleward deviation of the subtropical jet from its climatological position to superpose with the polar jet near its climatological position. These categories of jet superposition events comprise the spectrum of interactions that can occur between PV anomalies along the polar and subtropical waveguides prior to jet superpositions.

The climatological characteristics of events within these categories, and their associated synoptic-scale evolutions, are the focus for the remainder of the study.

3. Jet Superposition Event Type Characteristics

The monthly frequency of North American jet superposition events as a function of event type is shown in Fig. 3. Overall, jet superposition events are most frequent during the months of November and December, and taper off during the remainder of the cold season. This result is consistent with the findings of Christenson et al. (2017; their Fig. 6), whose analysis shows a broader spatial coverage of North American jet superpositions during November and December compared to January, February, and March. Figure 3 also indicates that subtropical dominant events (N=129) are favored by roughly a 3:2 margin compared to polar dominant events (N=80), suggesting that substantial poleward excursions of the subtropical jet to superpose with the polar jet are more common than the converse evolution. The largest disparity between polar dominant and subtropical dominant events occurs during November and December, when subtropical dominant events are the most frequent event type by a considerable margin. Hybrid events (N=117) are the most frequent event type during January, February, and March.

Figure 4 illustrates the spatial frequency of jet superposition events as a function of event type. Polar dominant events (Fig. 4a) are most frequent along the U.S./Mexico border and along the northern coast of the Gulf of Mexico. The branch of higher frequencies extending towards the northeast U.S. is representative of those polar dominant events that initially develop at low latitudes and propagate downstream within upper-tropospheric southwesterly flow. This jet propagation is further apparent considering the statistics provided in Table 1, where the third and fourth columns of Table 1 reveal the average change in latitude and longitude of the position of a jet superposition event centroid during its life span. Namely, the average polar dominant event develops at subtropical latitudes (e.g., 29.7°N; 102.0°W) and translates towards the northeast throughout its life span, consistent with the branch of higher frequencies that extend towards the northeast U.S in Fig. 4a. Hybrid events (Fig. 4b) are most frequent within a 5°-latitude band ranging from 35°N to 40°N, with the largest number of events situated over the southeastern U.S. and western North Atlantic. Hybrid events (34.5°N; 94.3°W) initially develop farther northeast of polar dominant events and translate in a more zonal direction compared to polar dominant events (Table 1).

Subtropical dominant events (Fig. 4c) are characterized by two separate frequency maxima centered on the eastern and western coasts of North America, respectively. Consequently, the average location of jet superposition for subtropical dominant events (46.7°N; 92.1°W) is not representative of the frequency distribution shown in Fig. 4c. This observation motivated partitioning subtropical dominant events into an "eastern" and "western" category based on the position of each individual event centroid relative to the 96°W meridian at the start of an event. A comparison of the relative frequencies of eastern and western subtropical dominant events shows that eastern events (N=76) are more common than western events (N=53). Furthermore, eastern (48.5°N; 71.2°W) and western (44.0°N; 122.1°W) subtropical dominant events develop at higher latitudes compared to polar dominant and hybrid events, and both types of subtropical dominant events translate in a southeastward direction following their development (Table 1). The latter result suggests that subtropical dominant events often develop at the apex of upper-tropospheric ridges and subsequently propagate downstream within upper-tropospheric northwesterly flow.

4. Jet Superposition Event Type Composites

Composite analyses were constructed for each jet superposition event type to examine the synoptic-scale flow evolution during the 48-h period prior to jet superposition. All composites were calculated by shifting the CFSR and OLR data for each event so that each individual event centroid was collocated with the average starting latitude and longitude for its corresponding event type (Table 1). All CFSR and OLR data were weighted by the cosine of latitude before they were shifted, and a weighted average of the shifted CFSR and OLR data was calculated at each grid point within a domain bounded in latitude from 10°N to 80°N and in longitude from 150°E to 10°W to construct the event composites. A two-sided Student's *t*-test was performed on the composite 250-hPa geopotential height, precipitable water, and mean sea level pressure anomalies to identify regions that are statistically distinct from climatology at the 99% confidence level (Wilks 2011). The primary focus of the forthcoming discussion is to determine the dynamical processes that facilitate the development of a steep, two-step tropopause structure during polar, eastern subtropical, and western subtropical dominant superpositions. Hybrid events are not considered further, as the dynamical processes facilitating superposition during those events can be conceptualized as a combination of the processes diagnosed during polar, eastern subtropical, and western subtropical dominant events.

a) Polar Dominant Events

48 h prior to superposition, a surface cyclone in the Gulf of Alaska is situated in a favorable region for synoptic-scale ascent beneath the poleward-exit region of a zonally-extended and poleward-shifted North Pacific jet stream (Figs. 5a,b). Perturbation upper-tropospheric ridges are located farther downstream over the eastern North Pacific and eastern Canada, respectively, and a perturbation upper-tropospheric trough is positioned over the

southwestern U.S. at this time. A weak surface cyclone is also in a favorable location for further development downstream of the southwestern U.S. trough and is associated with a zonally-oriented band of negative OLR anomalies. These OLR anomalies are suggestive of increased cloud cover along the developing warm-frontal boundary attendant to the surface cyclone (not shown).

The eastern North Pacific ridge amplifies 24 h prior to superposition in conjunction with lower-tropospheric warm-air advection and implied diabatic heating within the warm sector of the surface cyclone in the Gulf of Alaska (Figs. 5c,d). The axis of the eastern North Pacific ridge also exhibits a positive tilt at this time, indicating a preference for anticyclonic wave breaking to precede polar dominant superpositions. Anticyclonic wave breaking over the eastern North Pacific subsequently contributes to further amplification of the southwestern U.S. trough 24 h prior to superposition.

A maximum in 300-hPa geostrophic warm-air advection is situated downstream of the southwestern U.S. trough 24 h prior to superposition (Fig. 5c), implying that the thermally-indirect circulation within the exit region of the developing superposed jet is shifted equatorward so as to position ascent beneath the jet core (e.g., Shapiro 1981, 1982; Lang and Martin 2012, 2013). In response to a favorable environment for synoptic-scale ascent, the surface cyclone intensifies during the intervening 24-h period (Figs. 5b,d). Perturbation southerly geostrophic flow that accompanies the intensified surface cyclone subsequently results in the development of a corridor of anomalous precipitable water within the cyclone's warm sector (Fig. 5d). The collocation of precipitable water anomalies, negative OLR anomalies, and implied ascent within the surface cyclone's warm sector suggests that widespread precipitation accompanies the surface cyclone at this time. Consequently, implied diabatic heating and negative PV advection along the dynamic tropopause by the irrotational wind (not shown) in the vicinity of the surface cyclone contribute to an amplification of the downstream ridge over eastern North America by the time of superposition (Fig. 5e).

Strengthened 300-hPa geostrophic warm-air advection and enhanced flow curvature downstream of the deep upper-tropospheric trough over the southern Plains at the time of superposition imply that synoptic-scale ascent continues unabated in the vicinity of the surface cyclone during the 24-h period prior to superposition (Figs. 5c,e). As a result, the surface cyclone reaches maximum intensity at the time of superposition (Fig. 5f). Precipitable water anomalies and negative OLR anomalies in the vicinity of the surface cyclone also achieve their maximum magnitudes at this time, suggesting that precipitation maximizes in both intensity and areal coverage concurrently with the formation of a superposition. Any implied areas of precipitation associated with the surface cyclone are located exclusively downstream of the jet superposition event centroid, however (Fig. 5f). Consequently, implied diabatic heating and the strongest upper-tropospheric irrotational wind are located too far downstream to play a direct role in the formation of the two-step tropopause structure that accompanies polar dominant jet superpositions. These processes do play an *indirect* role in facilitating superposition, however, by contributing to the amplification of the upper-tropospheric ridge over eastern North America. Namely, downstream flow amplification slows the eastward translation speed of the upper-tropospheric trough over the southern Plains, allowing additional time for the jet superposition to develop at the base of the trough.

Upstream of the jet superposition centroid, the upper-tropospheric flow pattern is characterized by 300-hPa geostrophic cold-air advection that initially develops 24 h prior to superposition (Figs. 5c,e). The presence of geostrophic cold-air advection suggests that the thermally-direct circulation within the jet-entrance region is shifted equatorward so as to position descent beneath the jet core. Labeled the “Shapiro effect” by Rotunno et al. (1994), descent beneath the jet core is strongly conducive to upper-tropospheric frontogenesis and the concomitant development of a tropopause fold (i.e., Shapiro 1981, 1982; Keyser and Pecnick 1985; Keyser and Shapiro 1986; Rotunno et al. 1994; Schultz and Doswell 1999; Schultz and Sanders 2002; Lang and Martin 2012; Martin 2014; Winters and Martin 2016, 2017). Consequently, descent beneath the jet-entrance region appears to play a direct role in the formation of the steep, two-step tropopause structure associated with a polar dominant jet superposition.

To investigate this assertion more rigorously, a series of vertical cross sections were constructed upstream of the developing superposed jet and perpendicular to the jet axis 12 h prior to superposition (C–C’) and at the time of superposition (D–D’). Consistent with the presence of 300-hPa geostrophic cold-air advection, these cross sections highlight a region of focused descent beneath and poleward of the jet core 12 h prior to superposition (Fig. 6a) and at the time of jet superposition (Fig. 6b). This descent accounts for a large fraction of the positive PV advection diagnosed along the dynamic tropopause at both times and, consequently, for a downward penetration of high-PV air from the lower stratosphere during the 12-h period prior to superposition (Figs. 6a,b). The downward penetration of high-PV air completes the production of the steep, two-step tropopause structure (Fig. 6b) that must accompany the superposition.

The cross sections also highlight the presence of a strong cyclonic PV anomaly on the poleward side of the jet that intensifies in magnitude during the 12-h period prior to superposition (Figs. 6a,b). Notably, the cross sections only highlight a small, weak anticyclonic PV anomaly above 200 hPa on the equatorward side of the jet. Consequently, the anomalously strong wind speeds that accompany a polar dominant jet superposition are driven disproportionately by the nondivergent circulation that accompanies the polar cyclonic PV anomaly. The lack of a strong anticyclonic PV anomaly on the equatorward side of the jet is not surprising, given that this event type requires a superposition to develop at the climatological latitude of the subtropical jet. This result, however, indicates that knowledge of the creation and subsequent transport of polar cyclonic PV anomalies towards subtropical latitudes is essential towards diagnosing the development of a polar dominant jet superposition.

b) Eastern Subtropical Dominant Events

The composite large-scale flow pattern 48 h prior to an eastern subtropical dominant event features a zonally oriented upper-tropospheric trough-ridge couplet centered over eastern North America (Fig. 7a). A surface cyclone is favorably positioned within a region of synoptic-scale ascent immediately downstream of the upper-tropospheric trough and beneath the jet-entrance region, with a surface anticyclone located downstream of the upper-tropospheric ridge over the western North Atlantic (Fig. 7b). The longitudinal juxtaposition of the surface cyclone and anticyclone results in perturbation southerly geostrophic flow over eastern North America and the subsequent poleward transport of anomalous precipitable water into the region. The collocation of precipitable water anomalies and negative OLR anomalies in the vicinity of the surface cyclone's warm-frontal boundary implies that widespread precipitation likely accompanies the surface cyclone at this time. Diabatic heating and negative PV advection along the dynamic tropopause by the irrotational wind (not shown) that accompanies any implied areas of precipitation subsequently contribute to the observed amplification of the upper-tropospheric ridge over eastern North America during the following 24-h period (Figs. 7a,c).

24 h prior to superposition, 300-hPa geostrophic warm-air advection is diagnosed within

the entrance region of the developing superposed jet (Fig. 7c). The presence of geostrophic warm-air advection suggests that the thermally-direct circulation within the jet-entrance region is shifted poleward relative to the jet axis, positioning ascent directly beneath the jet core at this time (e.g., Shapiro 1981, 1982; Lang and Martin 2012, 2013). Consequently, the surface cyclone remains favorably located within a region of synoptic-scale ascent, which contributes to the intensification of the surface cyclone observed during the previous 24-h period (Figs. 7b,d). The intensification of both the surface cyclone and the downstream surface anticyclone compared to the prior time results in a strengthened zonal pressure gradient over eastern North America and intensified southerly geostrophic flow (Fig. 7d). This intensified southerly geostrophic flow leads to stronger poleward moisture transport and larger precipitable water anomalies within the surface cyclone's warm sector 24 h prior to superposition. The distribution of negative OLR anomalies at this time overlap the positions of the warm- and cold-frontal boundaries attendant to the surface cyclone (not shown), and the collocation of these OLR anomalies with anomalous moisture and implied ascent suggests that widespread precipitation persists on the equatorward side of the developing superposed jet.

Widespread precipitation, implied diabatic heating, and negative PV advection by the irrotational wind along the dynamic tropopause in the vicinity of the surface cyclone contribute to further amplification of the upper-tropospheric ridge over eastern North America by the time of jet superposition (Figs. 7e,f). Consequently, the subtropical waveguide is displaced anomalously poleward of its climatological position. While 300-hPa geostrophic warm-air advection persists along the jet axis at the time of superposition, areas of warm-air advection are now more focused in the jet-exit rather than in the jet-entrance region, as they were 24 h earlier (Figs. 7c,e). The presence of geostrophic warm-air advection in the jet-exit region suggests that the thermally-indirect circulation within the jet-exit region is shifted equatorward so as to promote continued ascent beneath the jet core (Fig. 7e). While the surface cyclone remains favorably aligned with this area of synoptic-scale ascent, the surface cyclone does not intensify during the 24-h period prior to superposition (Figs. 7d,f). Additionally, precipitable water anomalies and negative OLR anomalies have decreased in magnitude during the intervening 24-h period. Together, these observations imply that surface cyclogenesis and widespread precipitation tend to *lead* the development of eastern subtropical dominant jet superpositions, in contrast to polar dominant events.

Farther upstream, 300-hPa geostrophic cold-air advection is diagnosed within the jet-entrance region at the time of jet superposition (Fig. 7e). As discussed during polar dominant events, geostrophic cold-air advection within the jet-entrance region is indicative of descent beneath the jet core. This descent can subsequently contribute to the formation of the two-step tropopause structure that accompanies the jet superposition. To investigate the formation of the superposed jet's two-step tropopause structure further, a vertical cross section (E–E') is drawn immediately upstream of the jet superposition centroid and perpendicular to the jet axis. The evolution of the tropopause is investigated within this cross section both 12 h prior to superposition (Fig. 8a) and at the time of superposition (Fig. 8b).

Figure 8a depicts an area of ascent directly beneath the jet core 12 h prior to superposition, consistent with the presence of geostrophic warm-air advection along the jet axis and implied ascent along the surface cyclone's attendant frontal boundaries during the 24-h period prior to superposition (Figs. 7c,d). This ascent accounts for a large fraction of the negative PV advection diagnosed along the tropopause and acts to locally steepen the slope of the tropopause during the 12-h period prior to superposition (Figs. 8a,b). Furthermore, given that this ascent is occurring within an anomalously moist environment (Figs. 7d,f), diabatic heating contributes to the erosion of upper-tropospheric PV on the equatorward side of the jet during the 12-h period prior to superposition (Figs. 8a,b). In combination, these processes reveal the direct role that moist ascent plays during the production of eastern subtropical dominant superpositions through its contribution to a tropopause structure that is considerably steeper by the time of superposition. A narrow zone of descent also develops beneath the jet core at the time of superposition (Fig. 8b), in agreement with the geostrophic cold-air advection diagnosed within the jet-entrance region at this time (Fig. 7e). As in polar dominant events, this descent facilitates the downward transport of high-PV air from the lower stratosphere and contributes to the vertical depth of the resultant two-step tropopause structure that defines the jet superposition.

In contrast to polar dominant events (Figs. 6a,b), the cross sections shown in Figs. 8a,b indicate that the superposed jet is characterized by the horizontal juxtaposition of a polar cyclonic and a tropical anticyclonic PV anomaly during the 12-h period prior to superposition. This configuration of upper-tropospheric PV anomalies strongly resembles the conceptual model shown within Fig. 1c and indicates that the nondivergent circulations that accompany each PV anomaly add constructively to produce the anomalously strong wind speeds associated with eastern subtropical dominant jet superpositions. Consequently, knowledge of the creation, transport towards midlatitudes, and phasing of these two types of PV anomalies is critical towards correctly diagnosing the development of this jet superposition event type.

c) Western Subtropical Dominant Events

The development of western subtropical dominant events features the meridional juxtaposition of an anomalous upper-tropospheric trough at high latitudes and an anomalous ridge at subtropical latitudes 48 h prior to superposition, which results in a zonal extension of the

North Pacific jet stream (Fig. 9a). A surface cyclone is situated beneath the poleward-exit region of the jet, and is characterized by a corridor of anomalous precipitable water within perturbation southwesterly geostrophic flow on the cyclone's equatorward flank (Fig. 9b). The aspect ratio of this corridor of anomalous precipitable water strongly resembles the character of landfalling western U.S. atmospheric rivers (e.g., Newell et al. 1992; Zhu and Newell, 1998; Ralph et al. 2004, 2018, 2019; Cannon et al. 2018), and is collocated with broad regions of 300-hPa geostrophic warm-air advection and negative OLR anomalies. Consequently, the thermally-indirect circulation within the jet-exit region favors synoptic-scale ascent and the production of precipitation beneath the jet core in the vicinity of the Pacific Northwest at this time. Perturbation geostrophic winds near the surface are also oriented perpendicular to the west coast of North America, which suggests that orographic ascent likely contributes to the production of precipitation during these events, as well.

Areas of implied diabatic heating and negative PV advection by the irrotational wind along the dynamic tropopause are primarily confined equatorward of the double-jet structure (not shown), suggesting that these processes contribute to the amplification of the eastern North Pacific ridge 24 h prior to superposition (Fig. 9c). The upper-tropospheric trough poleward of the developing superposed jet also amplifies compared to the prior time, which leads to the acceleration of a jet streak west of the North American continent. The surface cyclone intensifies compared to the prior time beneath the poleward-exit region of the developing superposed jet, and is characterized by a stronger and more spatially-coherent corridor of anomalous precipitable water on its equatorward flank (Fig. 9d). The intersection of anomalous precipitable water with negative OLR anomalies, stronger 300-hPa geostrophic warm-air advection, and onshore lower-tropospheric geostrophic flow (Figs. 9c,d) suggests that widespread precipitation persists along the west coast of North America on the equatorward side of the developing superposed jet 24 h prior to superposition.

The perturbation upper-tropospheric trough and ridge near the west coast of North America achieve their maximum intensity at the time of jet superposition, resulting in further acceleration of wind speeds along the axis of the now superposed jet (Fig. 9e). The surface cyclone remains within a favorable environment for synoptic-scale ascent beneath the poleward-exit region of the superposed jet, with its corridor of anomalous precipitable water focused farther south than at prior times along the central California coast (Figs. 9e,f). Negative OLR anomalies and sea level pressure anomalies decrease in absolute magnitude, however, during the 24-h period prior to superposition (Figs. 9d,f). Similar to eastern subtropical dominant events, this observation suggests that surface cyclogenesis and widespread precipitation *lead* the formation of western subtropical dominant events.

As in polar and eastern subtropical dominant events, 300-hPa geostrophic cold-air advection develops within the entrance region of the jet at the time of superposition (Fig. 9e), indicating that the thermally-direct circulation in that location focuses descent beneath the jet core. To examine the impact of this descent as well as implied diabatic heating on the production of the jet's two-step tropopause structure, a cross section (F–F') is constructed immediately upstream of the jet superposition centroid and perpendicular to the jet axis. Figure 10a demonstrates that a focused region of ascent is present beneath the developing jet superposition 12 h prior to superposition, consistent with the presence of geostrophic warm-air advection along a considerable portion of the jet axis prior to superposition (Figs. 9c,e). This ascent accounts for a large fraction of the negative PV advection diagnosed along the tropopause and acts to locally steepen the tropopause. Additionally, given that this ascent is occurring within a corridor of anomalous moisture, implied diabatic heating that accompanies the ascent contributes to an erosion of upper-tropospheric PV on the equatorward side of the jet during the 12-h period prior superposition (Figs. 10a,b). The erosion of upper-tropospheric PV subsequently acts to further steepen the tropopause by the time of superposition.

A narrow zone of descent is diagnosed directly beneath the superposed jet core at the time of superposition (Fig. 10b). As in the previous event composites, this descent accounts for positive PV advection at the base of the tropopause break and, consequently, a downward penetration of high-PV air from the lower stratosphere. The downward transport of high-PV air from the lower stratosphere further steepens the tropopause and contributes to the formation of the two-step tropopause structure that prevails at the time of superposition. Both cross sections shown in Figs. 10a,b also demonstrate that the superposed jet is characterized by the meridional juxtaposition of a polar cyclonic and tropical anticyclonic PV anomaly near the tropopause. Consequently, the acceleration of wind speeds in the vicinity of the superposition results from the constructive interference between the nondivergent circulations that accompany each PV anomaly. Therefore, as in eastern subtropical dominant events, knowledge of the creation, transport towards midlatitudes, and phasing of these two PV anomalies is critical for correctly diagnosing the production of a western subtropical dominant event.

5. Conclusion

This study classifies North American jet superposition events into characteristic event types based on the relative deviation of the polar and subtropical jets from their respective climatological latitude bands, and investigates the dynamical mechanisms that facilitate the production of a steep, two-step tropopause structure during each jet superposition event type.

The dynamical evolutions associated with each jet superposition event type are summarized through a series of conceptual models presented in Fig. 11.

Polar dominant events (Fig. 11a) exhibit a preference for anticyclonic wave breaking over the eastern North Pacific during the 48-h period prior to jet superposition. Anticyclonic wave breaking subsequently facilitates the equatorward transport of a polar cyclonic PV anomaly towards subtropical latitudes and allows the polar jet to superpose with the subtropical jet near the climatological position of the subtropical jet. Surface cyclogenesis occurs primarily within the poleward-exit region of the jet and peaks in intensity concurrently with the development of the superposition. The surface cyclone features anomalous poleward moisture transport within its warm sector, and is likely associated with widespread precipitation that also reaches peak intensity and spatial coverage at the time of superposition. Given that surface cyclogenesis and areas of implied precipitation are located well downstream of the jet superposition, moist ascent does not play a direct role in the formation of the two-step tropopause structure that accompanies polar dominant events. Instead, upper-tropospheric geostrophic cold-air advection within the entrance region of the developing superposed jet is indicative of descent beneath the jet core. This descent is determined to play the primary role in facilitating the development of the superposed jet's two-step tropopause structure during polar dominant events.

In contrast to polar dominant events, surface cyclogenesis and implied precipitation *lead* the development of eastern subtropical dominant events (Fig. 11b). In particular, surface cyclogenesis and implied precipitation occur predominantly within the equatorward-entrance region of the developing superposed jet. Moist ascent, therefore, plays a direct role in the development of the superposed jet's two-step tropopause structure by locally steepening the tropopause via tilting and via the diabatic erosion of upper-tropospheric PV on the equatorward side of the jet. As in polar dominant events, upper-tropospheric geostrophic cold-air advection develops within the jet-entrance region during the 24-h period immediately preceding superposition and indicates descent beneath the jet core in that location. This descent acts to steepen the tropopause further by the time of superposition via the subduction of high-PV air from the lower stratosphere, thereby completing the formation of the superposed jet's two-step tropopause structure.

Western subtropical dominant events (Fig. 11c) are characterized by surface cyclogenesis that occurs beneath the poleward-exit region of the jet, rather than beneath the equatorward jet-entrance region as observed during eastern subtropical dominant events. The surface cyclone is accompanied by a zonally-oriented corridor of anomalous moisture that strongly resembles the character of a western U.S. atmospheric river. Widespread ascent and implied precipitation diagnosed along this corridor of anomalous moisture peak *prior* to the development of a jet superposition, as in eastern subtropical events, and play a direct role in the production of the superposed jet's two-step tropopause structure by steepening the tropopause locally via tilting and via the diabatic erosion of upper-tropospheric PV on the equatorward side of the jet. As observed during the other event types, upper-tropospheric geostrophic cold-air advection develops within the jet-entrance region by the time of superposition. Consequently, descent plays a critical role in completing the production of western subtropical dominant jet superpositions by contributing to the production of the superposed jet's two-step tropopause structure, as well.

The event types considered as part of this study reveal the varied roles that moist processes can play during the production of North American jet superpositions. Namely, surface cyclogenesis and implied precipitation appear to contribute directly to the formation of a two-step tropopause structure during subtropical dominant events, whereas surface cyclogenesis and implied precipitation develop concurrently with and downstream of polar dominant events. This difference motivates future work that investigates the relative importance of diabatic heating during observed jet superposition events. Of particular interest, is whether the omission of diabatic heating during the 48-h period prior to each jet superposition event type results in the successful formation of a jet superposition. It is hypothesized that subtropical dominant events are more sensitive to the omission of diabatic heating than polar dominant events, given the direct role that diabatic heating appears to play in restructuring the tropopause during that event type. The scrutiny of dry and full-physics simulations for select jet superposition events within each event type is one pathway through which to examine in greater detail the role that diabatic heating plays during jet superpositions.

A key result from this study is that descent beneath the entrance region of a developing jet superposition is a shared element regardless of the event type under consideration. This result motivates two critical research questions concerning the production of descent during jet superposition events. First, what fraction of the observed descent is due to across-front ageostrophic circulations that arise due to geostrophic frontogenesis within the confluent jet-entrance region (i.e., divergence of the across-front component of the **Q**-vector) versus along-front couplets of vertical motion that arise due to flow curvature and are of the scale of baroclinic waves (i.e., divergence of the along-front component of the **Q**-vector; e.g., Keyser et al. 1992; Martin 2006; Martin 2014)? The large-scale evolutions discussed in section 4 demonstrate that both of these processes are certain to operate within North American jet superposition environments. Second, what fraction of the observed descent within each event type can be attributed to the three-dimensional circulations that accompany upper-tropospheric PV anomalies along the polar and subtropical waveguides? The answer to the second question, in particular, is likely to reveal the relative influence that polar cyclonic and tropical anticyclonic PV anomalies have on the production of a superposed jet's two-step tropopause structure during each event type, and, consequently, determine the degree to which superpositions result from midlatitude or tropical dynamical processes.

North American jet superposition events during the cool season are most frequent during November and December, rather than during January and February as they are in the western North Pacific and northern Africa (Christenson et al. 2017; their Fig. 6). Given that North American jet superpositions are generally preceded by the development of a high-amplitude flow pattern, the frequency distribution of North American jet superposition events throughout the cold season may be related to the lower frequency of Rossby wave breaking events in the eastern North Pacific during the winter compared to the fall and spring (e.g., Abatzoglou and Magnusdottir 2006; Bowley et al. 2019). Additionally, prior case study work suggests that jet superpositions can form outside of the cold season (i.e., Christenson 2013; Winters and Martin 2014, 2016). Therefore, subsequent examinations of jet superposition events should modify the jet identification scheme employed within this study to identify superposition events that occur during the fall and spring. A comparison between jet superposition events across seasons has the potential to highlight the degree to which the dynamical processes and the types of sensible weather impacts that accompany jet superposition events vary as a function of season.

The composite analyses investigated in this study demonstrate that jet superpositions are often associated with surface cyclogenesis, and strongly resemble a dynamical and thermodynamic environment that is conducive to the production of widespread precipitation over North America (e.g., Moore et al. 2015; Moore et al. 2019). However, a cursory examination of individual events within each jet superposition event type indicates that some events are not necessarily associated with sensible weather within the near-jet environment that can be characterized as “high-impact”. Consequently, future work that differentiates between jet superposition environments that lead to high-impact weather events versus those that result in null events offers the potential to provide benefits to operational forecasts of high-impact weather. Finally, the development and subsequent downstream propagation of superposed jets can strongly reconfigure the large-scale flow pattern over the North Atlantic. Consequently, further understanding of the impacts that North American jet superpositions may impose on the downstream large-scale flow pattern may have important implications for operational forecasts of conditions in western Europe.

Acknowledgments

This work was supported by the National Science Foundation through an AGS Postdoctoral Research Fellowship (AGS-1624316) held at the University at Albany, State University of New York by ACW.

References

Abatzoglou, J. T., and G. Magnusdottir, 2006: Planetary wave breaking and nonlinear reflection: Seasonal cycle and interannual variability. *J. Climate*, **19**, 6139–6152, doi: 10.1175/JCLI3968.1.

Agustí-Panareda, A., C. D. Thorncroft, G. C. Craig, and S. L. Gray, 2004: The extratropical transition of Hurricane Irene (1999): A potential-vorticity perspective. *Quart. J. Roy. Meteor. Soc.*, **130**, 1047–1074, doi: 10.1256/qj.02.140.

Ahmadi-Givi, F., G. C. Craig, and R. S. Plant, 2004: The dynamics of a midlatitude cyclone with very strong latent-heat release. *Quart. J. Roy. Meteor. Soc.*, **130**, 295–323, doi: 10.1256/qj.02.226.

Archambault, H. M., L. F. Bosart, D. Keyser, and J. M. Cordeira, 2013: A climatological analysis of the extratropical flow response to recurving western North Pacific tropical cyclones. *Mon. Wea. Rev.*, **141**, 2325–2346, doi: 10.1175/MWR-D-12-00257.1.

Archambault, H. M., D. Keyser, L. F. Bosart, C. A. Davis, and J. M. Cordeira, 2015: A composite perspective of the extratropical flow response to recurving western North Pacific tropical cyclones. *Mon. Wea. Rev.*, **143**, 1122–1141, doi: 10.1175/MWR-D-14-00270.1.

Bowley, K. A., J. R. Gyakum, and E. H. Atallah, 2019: A new perspective toward cataloging Northern Hemisphere Rossby wave breaking on the dynamic tropopause. *Mon. Wea. Rev.*, **147**, 409–431, doi: 10.1175/MWR-D-18-0131.1.

Cannon, F., C. W. Hecht, J. M. Cordeira, and F. M. Ralph, 2018: Synoptic and mesoscale forcing of southern California extreme precipitation. *J. Geophys. Res.: Atmospheres*, **123**, 13714–13730, doi: 10.1029/2018JD029045.

Cavallo, S. M., and G. J. Hakim, 2009: Potential vorticity diagnosis of a tropopause polar cyclone. *Mon. Wea. Rev.*, **137**, 1358–1371, doi: 10.1175/2008MWR2670.1.

Cavallo, S. M., and G. J. Hakim, 2010: Composite structure of tropopause polar cyclones. *Mon. Wea. Rev.*, **138**, 3840–3857, doi: 10.1175/2010MWR3371.1.

Cavallo, S. M., and G. J. Hakim, 2012: Radiative impact on tropopause polar vortices over the Arctic. *Mon. Wea. Rev.*, **140**, 1683–1702, doi: 10.1175/MWR-D-11-00182.1.

Cavallo, S. M., and G. J. Hakim, 2013: Physical mechanisms of tropopause polar vortex intensity change. *J. Atmos. Sci.*, **70**, 3359–3373, doi: 10.1175/JAS-D-13-088.1.

Christenson, C. E., 2013: A synoptic-climatology of Northern Hemisphere polar and subtropical jet superposition events. M.S. thesis, University of Wisconsin–Madison, 62 pp.

Christenson, C. E., J. E. Martin, Z. J. Handlos, 2017: A synoptic climatology of Northern Hemisphere, cold season polar and subtropical jet superposition events. *J. Climate*, **30**, 7231–7246, doi: 10.1175/JCLI-D-16-0565.1.

Defant, F., and H. Taba, 1957: The threefold structure of the atmosphere and the characteristics of the tropopause. *Tellus,* **9**, 259–275, doi:10.3402/tellusa.v9i3.9112.

Fröhlich, L., P. Knippertz, A. H. Fink, and E. Hohberger, 2013: An objective climatology of tropical plumes. *J. Climate*, **26**, 5044–5060, doi: 10.1175/JCLI-D-12-00351.1.

Grams, C. M., H. Wernli, M. Böttcher, J. Čampa, U. Corsmeier, S. C. Jones, J. H. Keller, C.-J. Lenz, and L. Wiegand, 2011: The key role of diabatic processes in modifying the upper-tropospheric wave guide: A North Atlantic case-study. *Quart. J. Roy. Meteor. Soc.*, **137,** 2174–2193, doi: 10.1002/qj.891.

Grams, C. M., S. C. Jones, C. A. Davis, P. A. Harr, and M. Weissmann, 2013: The impact of Typhoon Jangmi (2008) on the midlatitude flow. Part I: Upper-level ridgebuilding and modification of the jet. *Quart. J. Roy. Meteor. Soc.,* **139,** 2148−2164, doi: 10.1002/qj.2091.

Grams, C. M., and H. M. Archambault, 2016: The key role of diabatic outflow in amplifying the midlatitude flow: A representative case study of weather systems surrounding western North Pacific extratropical transition. *Mon. Wea. Rev.*, **144**, 3847–3869, doi: 10.1175/MWR-D-15-0419.1.

Hakim, G. J., 2000: Climatology of coherent structures on the extratropical tropopause. *Mon. Wea. Rev.*, **128**, 385–406, doi: 10.1175/1520-0493%282000%29128<0385%3ACOCSOT>2.0.CO%3B2.

Hakim, G. J., L. F. Bosart, and D. Keyser, 1995: The Ohio Valley wave-merger cyclogenesis event of 25–26 January 1978. Part I: Multiscale case study. *Mon. Wea. Rev.*, **123**, 2663–2692, doi: 10.1175/1520-0493(1995)123<2663:TOVWMC>2.0.CO;2.

Hakim, G. J., D. Keyser, and L. F. Bosart, 1996: The Ohio Valley wave-merger cyclogenesis event of 25–26 January 1978. Part II: Diagnosis using quasigeostrophic potential vorticity inversion. *Mon. Wea. Rev.*, **124**, 2176–2205, doi: 10.1175/1520-0493(1996)124<2176:TOVWMC>2.0.CO;2.

Handlos, Z. J., and J. E. Martin, 2016: Composite analysis of large-scale environments conducive to west Pacific polar/subtropical jet superposition. *J. Climate*, **29**, 7145–7165, doi: 10.1175/JCLI-D-16-0044.1.

Held, I. M., 1975: Momentum transport by quasi-geostrophic eddies. *J. Atmos. Sci.*, **32**, 1494–1497, doi: 10.1175/ 1520-0469(1975)032,1494:MTBQGE.2.0.CO;2.

Held, I. M., and A. Y. Hou, 1980: Nonlinear axially symmetric circulations in a nearly inviscid atmosphere. *J. Atmos. Sci.*, **37**, 515–533, doi: 10.1175/1520-0469(1980)037<0515:NASCIA>2.0.CO;2.

Iskenderian, H., 1995: A 10-year climatology of Northern Hemisphere tropical cloud plumes and their composite flow patterns. *J. Climate*, **8**, 1630–1637, doi: 10.1175/1520-0442(1995)008<1630:AYCONH>2.0.CO;2.

Kalnay, E., and Coauthors, 1996: The NCEP/NCAR 40-Year Reanalysis Project. *Bull. Amer. Meteor. Soc.*, **77**, 437–470, doi: 10.1175/1520-0477(1996)077,0437:TNYRP.2.0.CO;2.

Keyser, D., and M. J. Pecnick, 1985: A two-dimensional primitive equation model of frontogenesis forced by confluence and horizontal shear. *J. Atmos. Sci.*, **42**, 1259–1282, doi: 10.1175/1520-0469(1985)042,1259:ATDPEM.2.0.CO;2.

Keyser, D., and M. A. Shapiro, 1986: A review of the structure and dynamics of upper-level frontal zones. *Mon. Wea. Rev.*, **114**, 452–499, doi: 10.1175/1520-0493(1986)114<0452:AROTSA>2.0.CO;2.

Keyser, D., B. D. Schmidt, and D. G. Duffy, 1992: Quasigeostrophic vertical motions diagnosed from along- and cross-isentrope components of the Q vector. *Mon. Wea. Rev.*, **120**, 731–741, doi: 10.1175/1520-0493%281992%29120<0731%3AQVMDFA>2.0.CO%3B2.

Kistler, R., and Coauthors, 2001: The NCEP–NCAR 50-Year Reanalysis: Monthly means CD-ROM and documentation. *Bull. Amer. Meteor. Soc.*, **82**, 247–267, doi: 10.1175/ 1520-0477(2001)082,0247:TNNYRM.2.3.CO;2.

Koteswaram, P., 1953: An analysis of the high tropospheric wind circulation over India in winter. *Indian J. Meteor. Geophys.*, **4**, 13–21.

Koteswaram, P., and S. Parthasarathy, 1954: The mean jet stream over Indian in the pre-monsoon and post-monsoon seasons and vertical motions associated with subtropical jet streams. *Indian J. Meteor. Geophys.*, **5**, 138–156.

Krishnamurti, T. N., 1961: The subtropical jet stream of winter. *J. Meteor.*, **18**, 172–191, doi: 10.1175/1520-0469(1961)018<0172:TSJSOW>2.0.CO;2.

Lang, A. A., and J. E. Martin, 2012: The structure and evolution of lower stratospheric frontal zones. Part I: Examples in northwesterly and southwesterly flow. *Quart. J. Roy. Meteor. Soc.*, **138**, 1350–1365, doi: 10.1002/qj.843.

Lang, A. A., and J. E. Martin, 2013: The structure and evolution of lower stratospheric frontal zones: Part II: The influence of tropospheric ascent on lower stratospheric frontal development. *Quart. J. Roy. Meteor. Soc.*, **139**, 1798–1809, doi: 10.1002/qj.2074.

Lee, S., and H.-K. Kim, 2003: The dynamical relationship between subtropical and eddy-driven jets. *J. Atmos. Sci.*, **60**, 1490–1503, doi: 10.1175/1520-0469%282003%29060<1490%3ATDRBSA>2.0.CO%3B2.

Liebmann, B., and C. A. Smith, 1996: Description of a complete (interpolated) outgoing longwave radiation dataset. *Bull. Amer. Meteor. Soc.*, **77**, 1275–1277.

Loewe, F., and V. Radok, 1950: A meridional aerological cross section in the southwest Pacific. *J. Meteor.*, **7**, 58–65, doi: 10.1175/1520-0469(1950)007<0058:AMACSI>2.0.CO;2.

Martin J. E., 2006. The role of shearwise and transverse quasigeostrophic vertical motions in the midlatitude cyclone life cycle. *Mon. Wea. Rev.*, **134**, 1174–1193, doi: 10.1175/MWR3114.1.

Martin, J. E., 2014: Quasi-geostrophic diagnosis of the influence of vorticity advection on the development of upper level jet-front systems. *Quart. J. Roy. Meteor. Soc.*, **140**, 2658–2671, doi: 10.1002/qj.2333.

Martius, O., C. Schwierz, and H. C. Davies, 2010: Tropopause-level waveguides. *J. Atmos. Sci.*, **67**, 866–879, doi: 10.1175/2009JAS2995.1.

McTaggart-Cowan, R., J. R. Gyakum, and M. K. Yau, 2001: Sensitivity testing of extratropical transitions using potential vorticity inversions to modify initial conditions: Hurricane Earl case study. *Mon. Wea. Rev.*, **129**, 1617–1636, doi: 10.1175/1520-0493%282001%29129<1617%3ASTOETU>2.0.CO%3B2.

McTaggart-Cowan, R., J. R. Gyakum, and M. K. Yau, 2004: The impact of tropical remnants on extratropical cyclogenesis: Case study of Hurricanes Danielle and Earl (1998). *Mon. Wea. Rev.*, **132**, 1933–1951, doi: 10.1175/1520-0493%282004%29132<1933%3ATIOTRO>2.0.CO%3B2.

McTaggart-Cowan, R., L. F. Bosart, J. R. Gyakum, and E. H. Atallah, 2007: Hurricane Katrina (2005). Part II: Evolution and hemispheric impacts of a diabatically generated warm pool. *Mon. Wea. Rev.*, **135**, 3927–3949, doi: 10.1175/2007MWR2096.1.

McWilliams, J. C., and J. H. S. Chow, 1981: Equilibrium geostrophic turbulence I: Reference solution in a β-plane channel. *J. Phys. Oceanogr.*, **11**, 921–949, doi: 10.1175/1520-0485(1981)011,0921:EGTIAR.2.0.CO;2.

Mohri, K., 1953: On the fields of wind and temperature over Japan and adjacent waters during winter of 1950–1951. *Tellus*, **5**, 340–358, doi: 10.3402/tellusa.v5i3.8582.

Moore, B. J., P. J. Neiman, F. M. Ralph, and F. E. Barthold, 2012: Physical processes associated with heavy flooding rainfall in Nashville, Tennessee, and vicinity during 1–2 May 2010:

The role of an atmospheric river and mesoscale convective systems. *Mon. Wea. Rev.*, **140**, 358–378, doi: 10.1175/MWR-D-11-00126.1.

Moore, B. J., K. M. Mahoney, E. M. Sukovich, R. Cifelli, and T. M. Hamill, 2015: Climatology and environmental characteristics of extreme precipitation events in the southeastern United States. *Mon. Wea. Rev.*, **143**, 718–741, doi: 10.1175/MWR-D-14-00065.1.

Moore, B. J., D. Keyser, and L. F. Bosart, 2019: Linkages between extreme precipitation events in the central and eastern United States and Rossby wave breaking. *Mon. Wea. Rev.*, **147**, 3327–3349, doi: 10.1175/MWR-D-19-0047.1.

Namias, J., and P. F. Clapp, 1949: Confluence theory of the high tropospheric jet stream. *J. Meteor.*, **6**, 330–336, doi: 10.1175/1520-0469(1949)006<0330:CTOTHT>2.0.CO;2.

Newell, R. E., N. E. Newell, Y. Zhu, and C. Scott, 1992: Tropospheric rivers?—A pilot study. *Geophys. Res. Lett.*, **19**, 2401–2404, doi: 10.1029/92GL02916.

Newton, C. W., 1954: Frontogenesis and frontolysis as a three-dimensional process. *J. Meteor.*, **11**, 449–461, doi: 10.1175/1520-0469(1954)011<0449:FAFAAT>2.0.CO;2.

Palmén, E., and C. W. Newton, 1948: A study of the mean wind and temperature distribution in the vicinity of the polar front in winter. *J. Meteor.*, **5**, 220–226, doi: 10.1175/1520-0469(1948)005<0220:ASOTMW>2.0.CO;2.

Palmén, E., and C. W. Newton, 1969: *Atmospheric Circulation Systems: Their Structure and Physical Interpretation*. Academic Press, 603 pp.

Panetta, R. L., 1993: Zonal jets in wide baroclinically unstable regions: Persistence and scale selection. *J. Atmos. Sci.*, **50**, 2073–2106, doi: 10.1175/1520-0469(1993)050,2073:ZJIWBU.2.0.CO;2.

Pyle, M. E., D. Keyser, and L. F. Bosart, 2004: A diagnostic study of jet streaks: Kinematic signatures and relationship to coherent tropopause disturbances. *Mon. Wea. Rev.*, **132**, 297–319, doi: 10.1175/1520-0493(2004)132<0297:ADSOJS>2.0.CO;2.

Ralph, F. M., P. J. Neiman, and G. A. Wick, 2004: Satellite and CALJET aircraft observations of atmospheric rivers over the eastern North Pacific Ocean during the winter of 1997/98. *Mon. Wea. Rev.*, **132**, 1721–1745, doi: 10.1175/1520-0493(2004)132<1721:SACAOO>2.0.CO;2.

Ralph, F. M., M. D. Dettinger, M. M. Cairns, T. J. Galarneau, and J. Eylander, 2018: Defining "atmospheric river": How the *Glossary of Meteorology* helped resolve a debate. *Bull. Amer. Meteor. Soc.*, **99**, 837–839, doi: 10.1175/BAMS-D-17-0157.1

Ralph, F. M., and Coauthors, 2019: A scale to characterize the strength of impacts of atmospheric rivers. *Bull. Amer. Meteor. Soc.*, **100**, 269–289, doi: 10.1175/BAMS-D-18-0023.1.

Rhines, P. B., 1975: Waves and turbulence on a beta-plane. *J. Fluid Mech.*, **69**, 417–433, doi: 10.1017/S0022112075001504.

Riehl, H., 1962: Jet streams of the atmosphere. Dept. of Atmospheric Science Tech. Rep. 32, Colorado State University, Fort Collins, CO, 117 pp.

Rotunno, R., W. C. Skamarock, and C. Snyder, 1994: An analysis of frontogenesis in numerical simulations of baroclinic waves. *J. Atmos. Sci.*, **51**, 3373–3398, doi: 10.1175/1520-0469(1994)051,3373:AAOFIN.2.0.CO;2

Roundy, P. E., K. MacRitchie, J. Asuma, and T. Melino, 2010: Modulation of the global atmospheric circulation by combined activity in the Madden–Julian oscillation and the El

Niño–Southern Oscillation during boreal winter. *J. Climate*, **23**, 4045–4059, doi: 10.1175/2010JCLI3446.1.

Saha, S., and Coauthors, 2010: The NCEP Climate Forecast System Reanalysis. *Bull. Amer. Meteor. Soc.*, **91**, 1015–1057, doi: 10.1175/2010BAMS3001.1.

Schultz, D. M., and C. A. Doswell III, 1999: Conceptual models of upper-level frontogenesis in south-westerly and north-westerly flow. *Quart. J. Roy. Meteor. Soc.*, **125**, 2535–2562, doi: 10.1002/qj.49712555910.

Schultz, D. M., and F. Sanders, 2002: Upper-level frontogenesis associated with the birth of mobile troughs in northwesterly flow. *Mon. Wea. Rev.*, **130**, 2593–2610, doi: 10.1175/1520-0493 (2002)130,2593:ULFAWT.2.0.CO;2.

Shapiro, M. A., 1981: Frontogenesis and geostrophically forced secondary circulations in the vicinity of jet stream-frontal zone systems. *J. Atmos. Sci.*, **38**, 954–973, doi: 10.1175/1520-0469(1981)038<0954:FAGFSC>2.0.CO;2.

Shapiro, M. A., 1982: *Mesoscale weather systems of the central United States.* CIRES, 78 pp.

Shapiro, M. A., T. Hampel, and A. J. Krueger, 1987: The Arctic tropopause fold. *Mon. Wea. Rev.*, **115**, 444–454, doi: 10.1175/1520-0493(1987)115,0444:TATF.2.0.CO;2.

Shapiro, M. A., and D. Keyser, 1990: Fronts, jet streams, and the tropopause. *Extratropical Cyclones: The Erik Palmén Memorial Volume*, C. Newton and E. O. Holopainen, Eds., Amer. Meteor. Soc., 167–191.

Son, S.-W., and S. Lee, 2005: The response of westerly jets to thermal driving in a primitive equation model. *J. Atmos. Sci.*, **62**, 3741–3757, doi: 10.1175/JAS3571.1.

Starr, V. P., 1948: An essay on the general circulation of the earth's atmosphere. *J. Meteor.*, **5**, 39–43.

Sutcliffe, R. C., and J. K. Bannon, 1954: Seasonal changes in the upper-air conditions in the Mediterranean Middle East area. *Proc. Int. Association of Meteorology*, Rome, Italy, Int. Union of Geodesy and Geophysics. 322–334.

Wilks, D. S., 2011: Statistical Methods in the Atmospheric Sciences. 3rd ed. Elsevier, 676 pp.

Winters, A. C., and J. E. Martin, 2014: The role of a polar/subtropical jet superposition in the May 2010 Nashville flood. *Wea. Forecasting*, **29**, 954–974, doi: 10.1175/WAF-D-13-00124.1.

Winters, A. C., and J. E. Martin, 2016: Synoptic and mesoscale processes supporting vertical superposition of the polar and subtropical jets in two contrasting cases. *Quart. J. Roy. Meteor. Soc.*, **142**, 1133–1149, doi: 10.1002/qj.2718.

Winters, A. C., and J. E. Martin, 2017: Diagnosis of a North American polar–subtropical jet superposition employing piecewise potential vorticity inversion. *Mon. Wea. Rev.*, **145**, 1853–1873, doi: 10.1175/MWR-D-16-0262.1.

Yeh, T. C., 1950: The circulation of the high troposphere over China in the winter of 1945–46. *Tellus*, **2**, 173–183, doi: 10.3402/tellusa.v2i3.8548.

Zhu, Y., and R. E. Newell, 1998: A proposed algorithm for moisture fluxes from atmospheric rivers. *Mon. Wea. Rev.*, **126**, 725–735, doi: 10.1175/1520-0493(1998)126<0725:APAFMF>2.0.CO;2.

Tables

Jet Superposition Characteristics				
	Avg. Starting Latitude	Avg. Starting Longitude	Avg. ΔLatitude	Avg. ΔLongitude
Polar Dominant (N = 80)	29.7°N	102.0°W	+3.42°	+12.25°
Hybrid (N=117)	34.5°N	94.3°W	+0.85°	+11.20°
Subtropical Dominant (N=129)	46.7°N	92.1°W	–0.96°	+12.32°
East Subtropical Dominant (N=76)	48.5°N	71.2°W	–1.13°	+9.56°
West Subtropical Dominant (N=53)	44.0°N	122.1°W	–0.78°	+15.10°

TABLE 1. Average characteristics of jet superposition events as a function of event type. These characteristics include the average starting latitude and longitude at which jet superpositions develop for each event type, and the average change (Δ) in latitude and longitude of a jet superposition centroid during the life span of each event type.

Figures

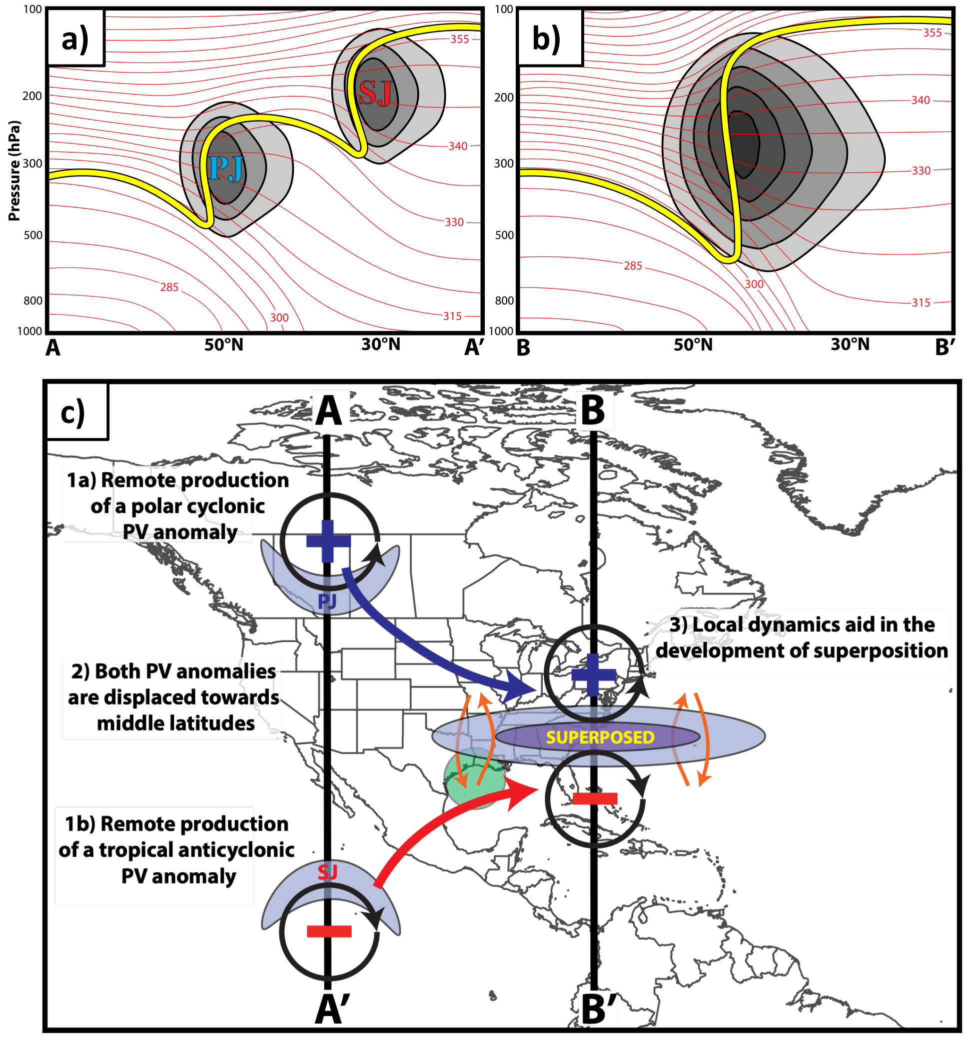

FIG. 1. (a) Idealized cross section along A–A′, as indicated in (c), through separate polar and subtropical jets. Wind speed is shaded in gray with darker shades of gray identifying stronger wind speeds, potential temperature is contoured in red every 5 K, the 2-PVU contour is drawn in yellow to highlight the structure of the dynamic tropopause, and the polar jet (PJ) and subtropical jet (SJ) are labeled accordingly. (b) As in (a), but for an idealized cross section along B–B′, as indicated in (c), through a jet superposition. (c) Conceptual model summarizing the development of a jet superposition. The orange arrows depict the branches of an across-front ageostrophic circulation, the green circle identifies an area of widespread precipitation, and the plus (minus) sign corresponds to the center of a polar cyclonic (tropical anticyclonic) PV anomaly, with the blue (red) arrow indicating the movement of that particular PV anomaly toward middle latitudes. The purple fill pattern corresponds to isotachs, with the darker shade of purple identifying stronger wind speeds. The locations of the polar jet (PJ), subtropical jet (SJ), and superposed jet are labeled accordingly. The locations of the cross sections, A–A′ and B–B′, examined in (a) and (b), respectively, are indicated by thick black lines. Figure and caption adapted from Winters and Martin (2017; their Fig. 2).

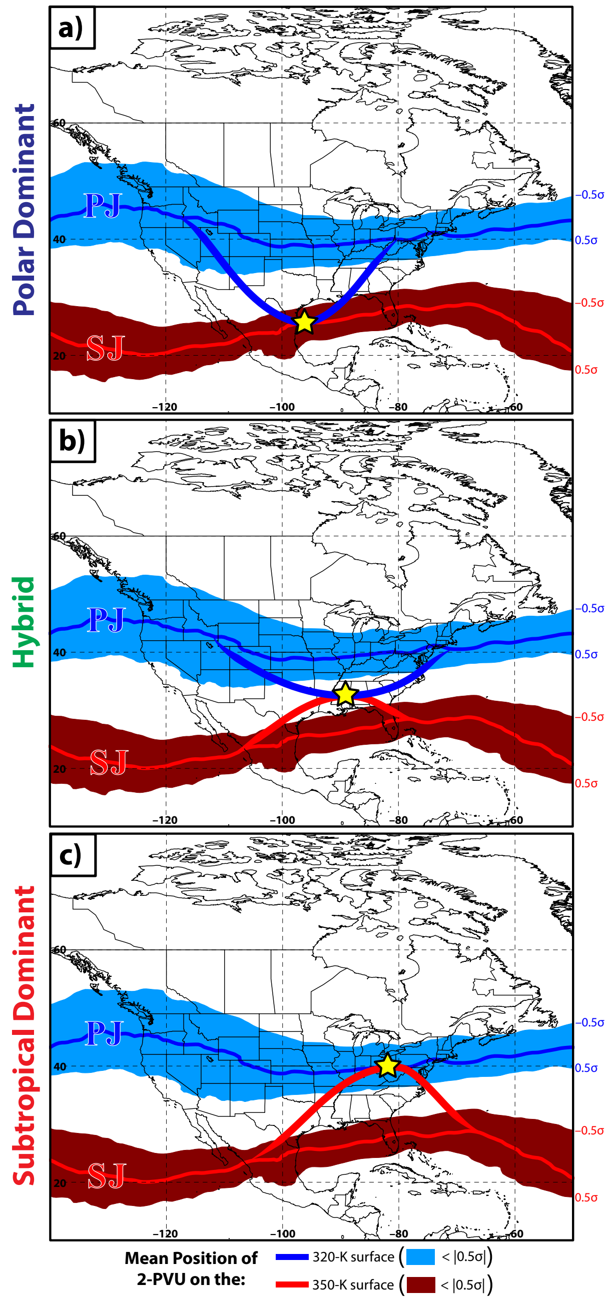

FIG. 2. The mean position of the 2-PVU contour on the 320-K and 350-K isentropic surfaces at 0000 UTC 1 January is indicated by the thin blue and red line, respectively, and represents the mean position of the polar (PJ) and subtropical (SJ) waveguides. Shaded areas bounding each mean 2-PVU contour indicate locations at which an observation of 2-PVU on that particular isentropic surface would represent a standardized PV anomaly with a magnitude less than 0.5. Hypothetical deviations of the 2-PVU contour from its mean position on each isentropic surface that result in the formation of (a) a polar dominant jet superposition event (yellow star) are indicated by the thick blue and red contours. (b) As in (a), but for a hybrid event. (c) As in (a), but for a subtropical dominant event.

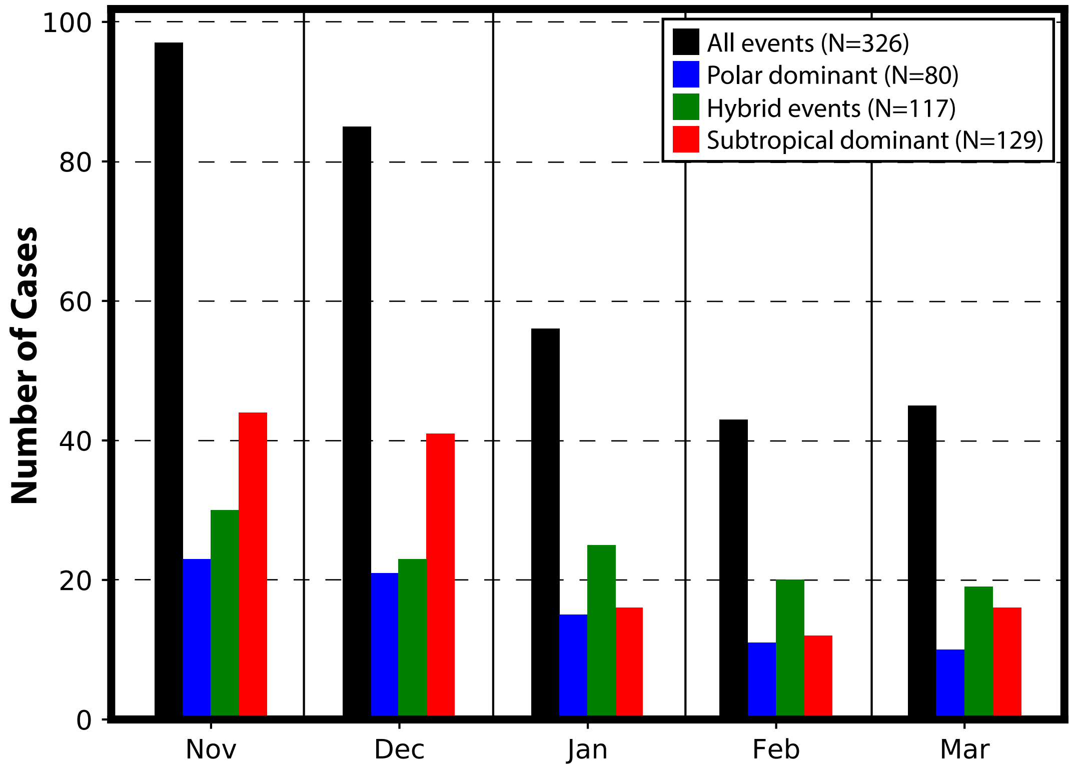

FIG. 3. Monthly frequency of jet superposition events as a function of event type.

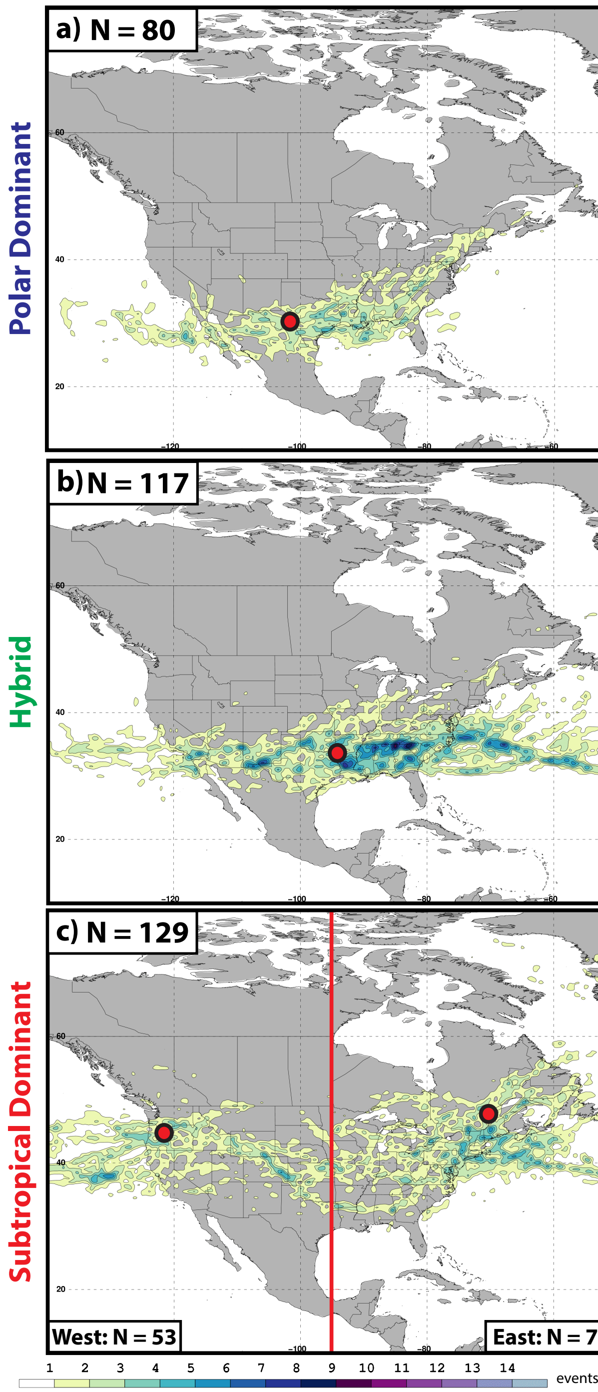

FIG. 4. (a) The spatial frequency of polar dominant jet superposition events is shaded according to the legend. The red circle represents the average starting latitude and longitude for polar dominant events, as indicated in Table 1. (b) As in (a), but for hybrid events. (c) As in (a) but for subtropical dominant events. The vertical red bar in (c) is used to illustrate the partition of subtropical dominant events into an eastern and a western category. The red dot to the east (west) of the vertical red line in (c) indicates the average location of superposition for eastern (western) subtropical dominant events.

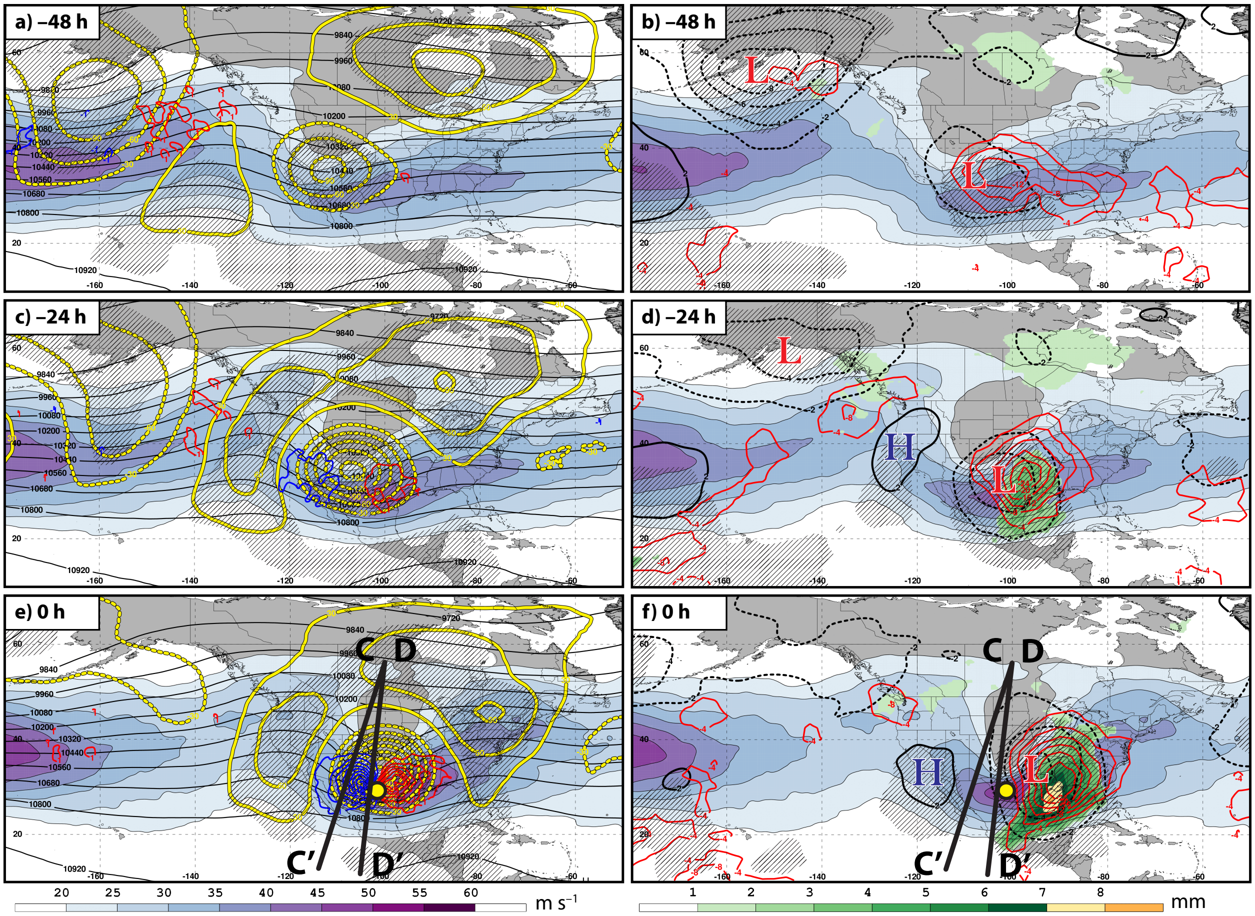

FIG. 5. Composite large-scale flow evolution prior to the initiation of a polar dominant jet superposition event. (left) 250-hPa geopotential height is contoured in black every 120 m, 250-hPa geopotential height anomalies are contoured in solid and dashed yellow every 30 m for positive and negative values, respectively, 250-hPa wind speed is shaded in m s^{-1} according to the legend, and 300-hPa geostrophic cold- (warm-) air advection is contoured in blue (red) every 1×10^{-4} K s^{-1} for (a) 48 h, (c) 24 h, and (e) 0 h prior to jet superposition. Hatched areas represent locations where the 250-hPa geopotential height anomalies are statistically distinct from climatology at the 99% confidence level. (right) 250-hPa wind speed is shaded in m s^{-1} according to the legend, mean sea level pressure anomalies are contoured in solid and dashed black every 2 hPa for positive and negative values, respectively, negative OLR anomalies are contoured in red every 4 W m^{-2}, and precipitable water anomalies are shaded in mm according to the legend at locations in which they are statistically distinct from climatology at the 99% confidence level for (b) 48 h, (d) 24 h, and (f) 0 h prior to jet superposition. Hatched areas represent locations where the mean sea level pressure anomalies are statistically distinct from climatology at the 99% confidence level. The red "L"s and blue "H"s identify the locations of surface cyclones and anticyclones. The yellow dot in (e) and (f) corresponds to the average location of jet superposition and the vertical cross sections, C–C′ and D–D′, in (e) and (f) are examined further in Figs. 6a,b, respectively.

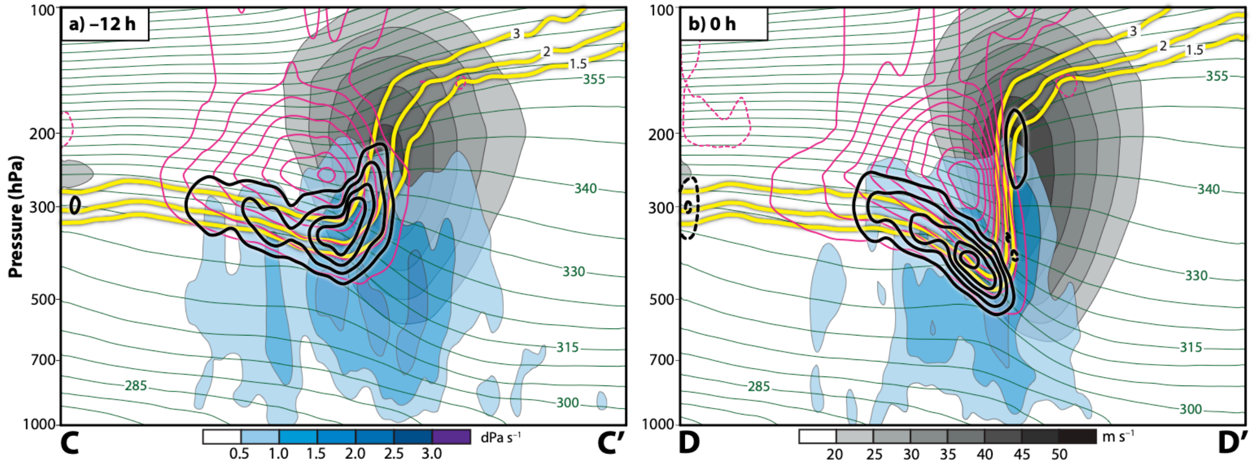

FIG. 6. (a) Cross section along C–C′, as indicated in Figs. 5e,f, 12 h prior to a polar dominant jet superposition event. Potential temperature is contoured in green every 5 K, wind speed (m s^{-1}) is shaded in gray according to the legend, positive (negative) PV anomalies are contoured in solid (dashed) magenta contours every 0.5 PVU, the 1.5, 2-, and 3-PVU contours are indicated in yellow, positive PV advection due to the divergent circulation (i.e., the sum of the irrotational wind and the vertical motion) is contoured in solid black contours every 0.5×10^{-5} PVU s^{-1}, and descent (dPa s^{-1}) is shaded in blue according to the legend. (b) As in (a), but for the cross section along D–D′, as indicated in Figs. 5e,f, 0 h prior to a polar dominant jet superposition event. Negative PV advection due to the divergent circulation is contoured in dashed black contours in (b) every -0.5×10^{-5} PVU s^{-1}

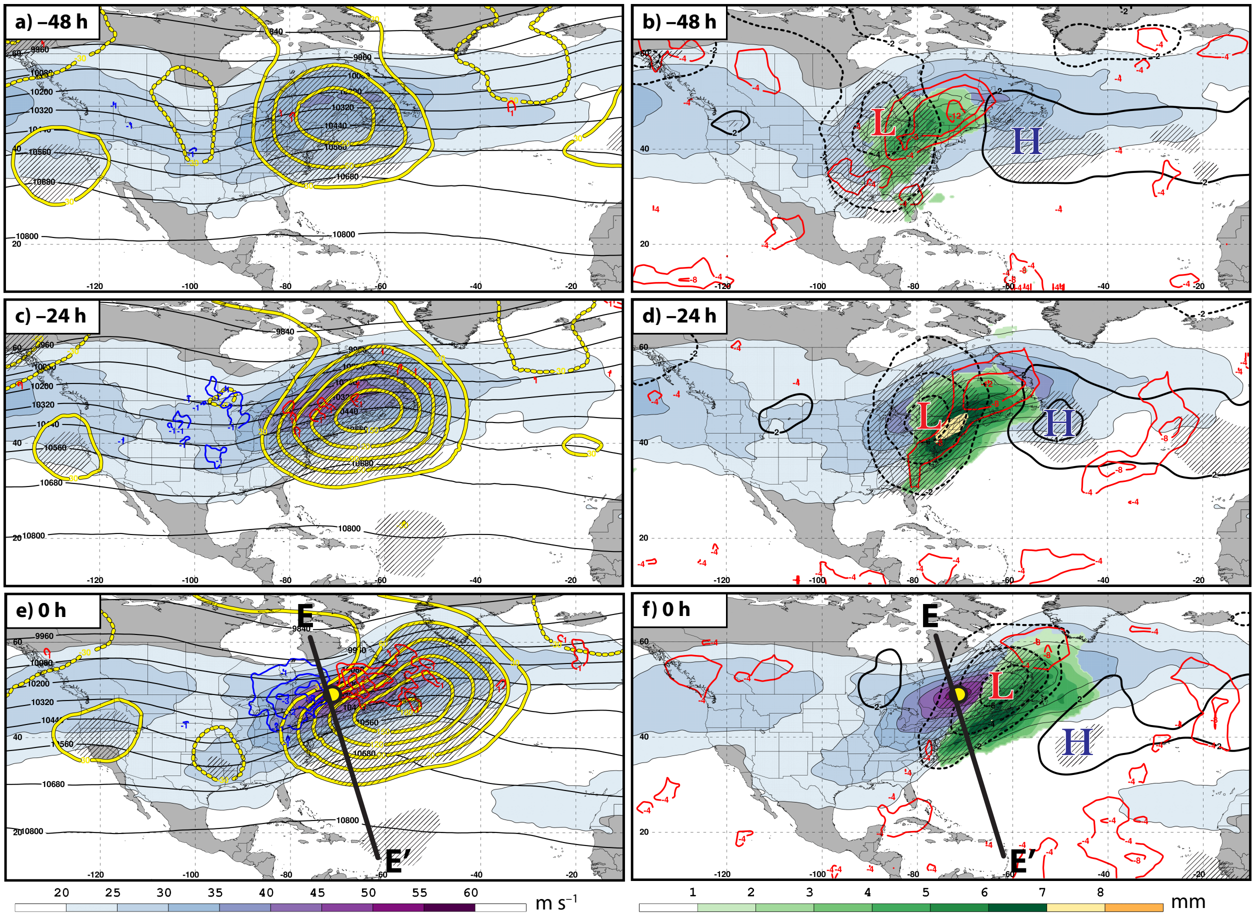

FIG. 7. Composite large-scale flow evolution prior to the initiation of an eastern subtropical dominant jet superposition event. All conventions are identical to those in Fig. 5.

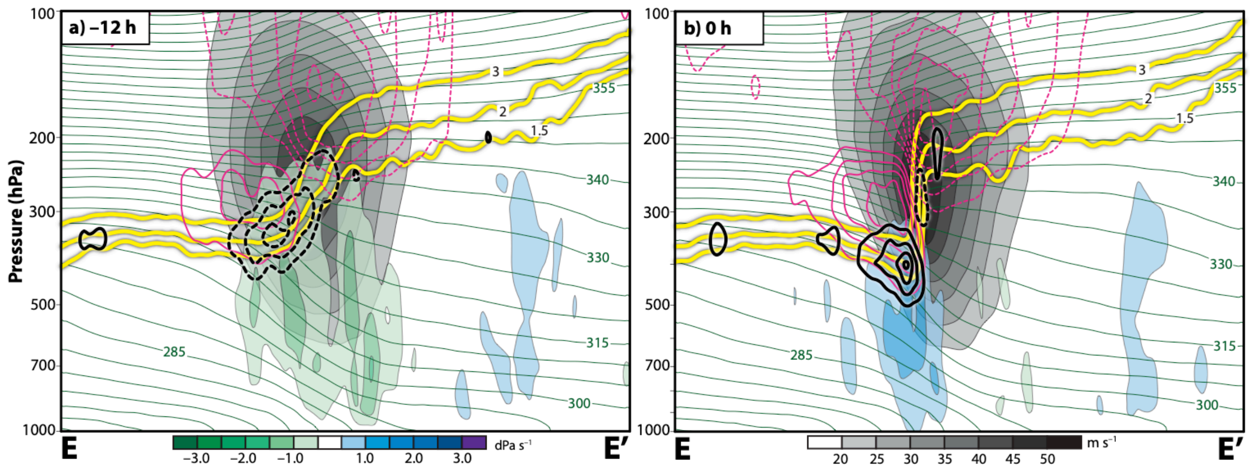

FIG. 8. (a) Cross section along E–E′, as indicated in Figs. 7e,f, 12 h prior to an eastern subtropical dominant jet superposition event. Potential temperature is contoured in green every 5 K, wind speed (m s^{-1}) is shaded in gray according to the legend, positive (negative) PV anomalies are contoured in solid (dashed) magenta contours every 0.5 PVU, the 1.5, 2-, and 3-PVU contours are indicated in yellow, positive (negative) PV advection due to the divergent circulation is contoured in solid (dashed) black contours every 0.5×10^{-5} PVU s^{-1}, and vertical motion (dPa s^{-1}) is shaded in blue and green according to the legend for descent and ascent, respectively. (b) As in (a), but for the cross section along E–E′, as indicated in Figs. 7e,f, 0 h prior to an eastern subtropical dominant jet superposition event.

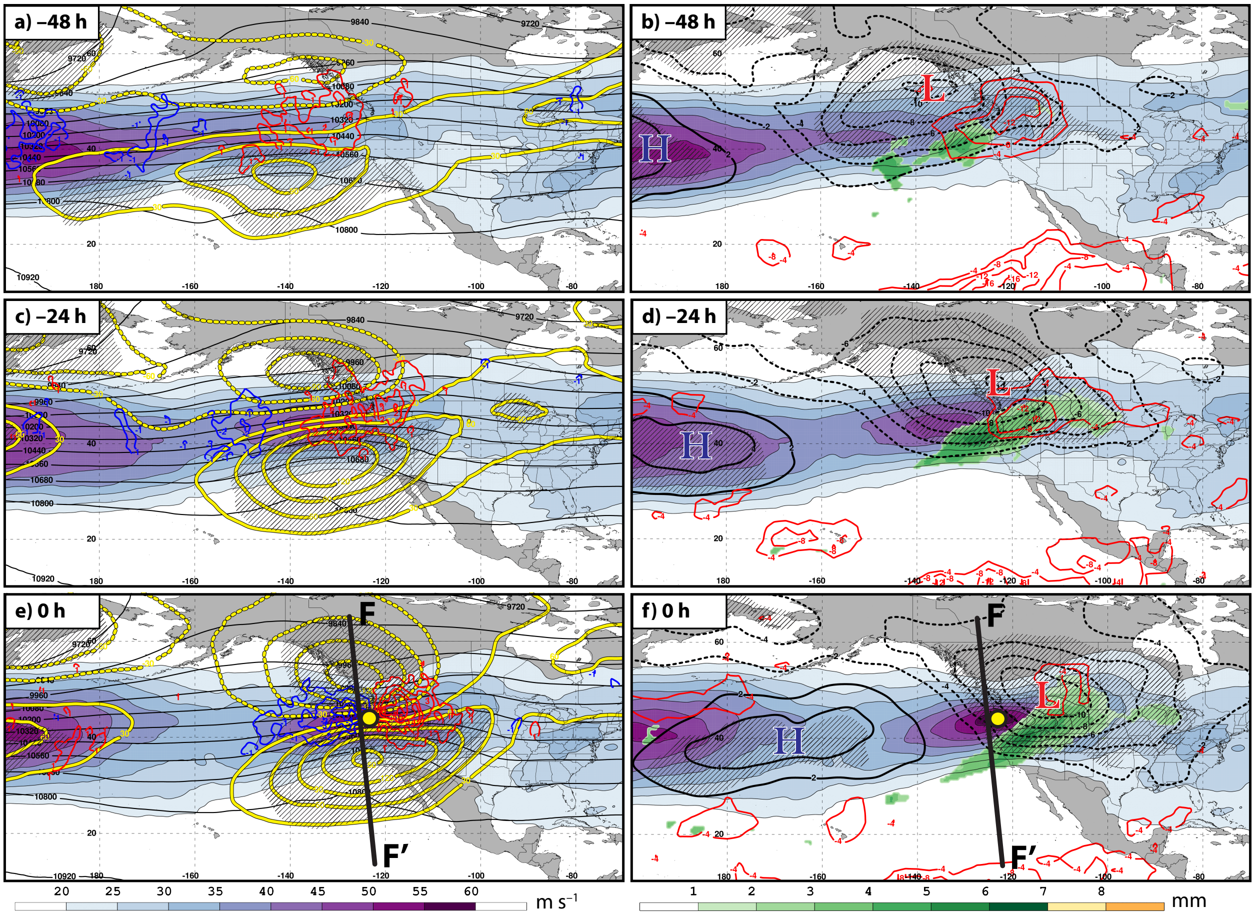

FIG. 9. Composite large-scale flow evolution prior to the initiation of a western subtropical dominant jet superposition event. All conventions are identical to those in Fig. 5.

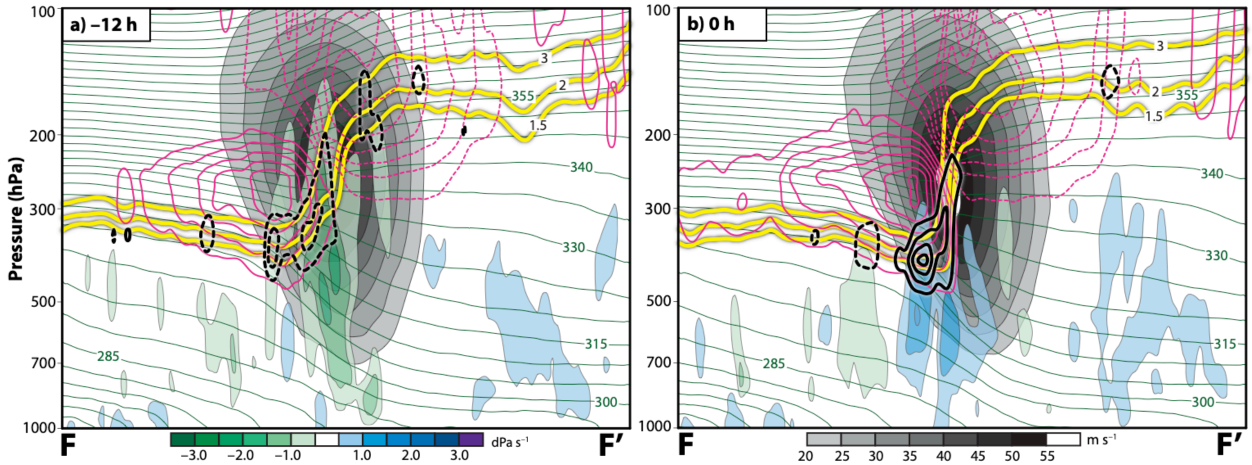

FIG. 10. (a) Cross section along F–F′, as indicated in Figs. 9e,f, 12 h prior to a western subtropical dominant jet superposition event. All conventions are identical to those in Fig. 8. (b) As in (a), but for the cross section along F–F′, as indicated in Figs. 9e,f, 0 h prior to a western subtropical dominant jet superposition event.

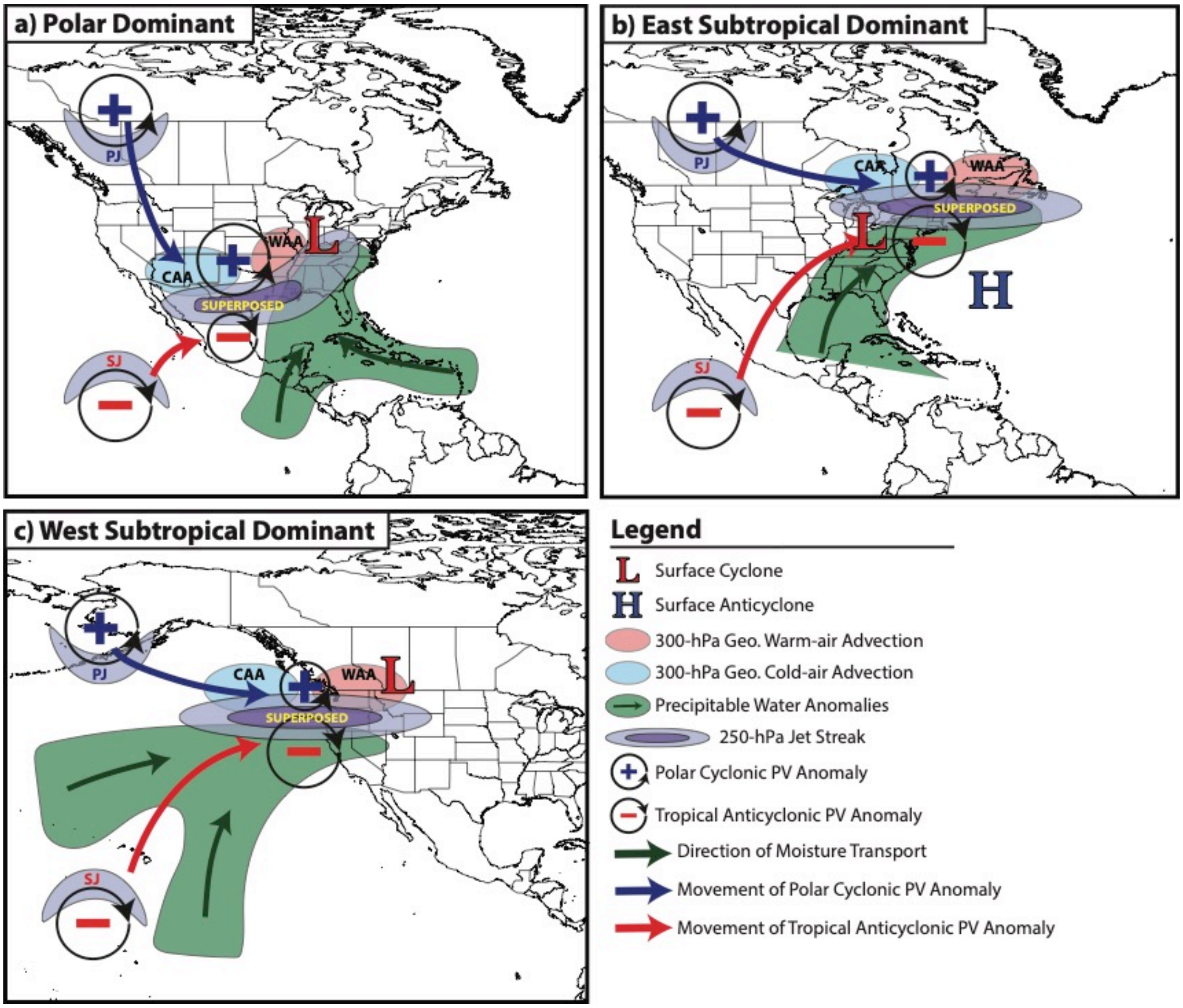

FIG. 11. Conceptual models for the development of (a) polar dominant, (b) eastern subtropical dominant, and (c) western subtropical dominant jet superposition events.